Supplementary information

Supplementary Figures

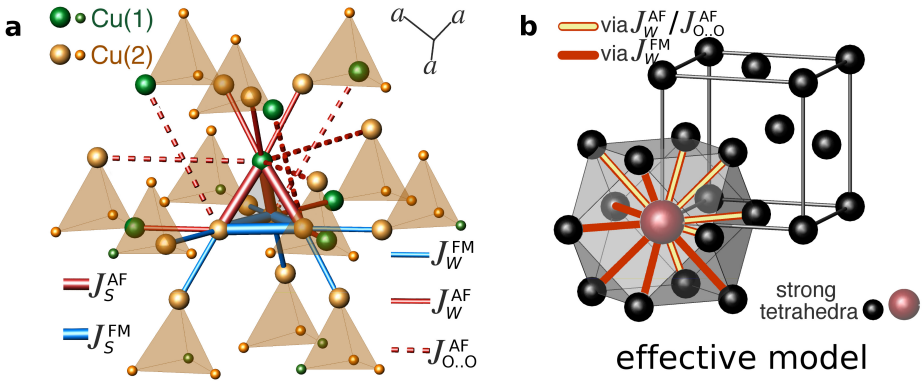

Supplementary Figure 1: **Microscopic magnetic model and the effective model**. **a**, microscopic magnetic model is based on five leading couplings: J_W^{FM}, J_S^{AF}, J_S^{FM}, J_W^{AF}, and $J_{\mathrm{O...O}}^{\mathrm{AF}}$. Strong tetrahedra are shaded. J_S^{AF} and J_S^{FM} are shown only for the central strong tetrahedron. **b**, effective model with two different types of ferromagnetic effective couplings: via $J_W^{\mathrm{AF}}/J_{\mathrm{O...O}}^{\mathrm{AF}}$ and via J_W^{FM} (compare with **a**).

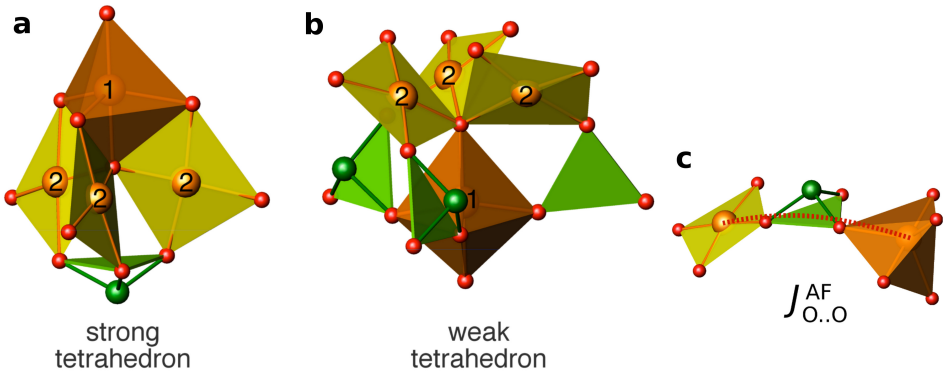

Supplementary Figure 2: **Structural building blocks of Cu_2OSeO_3.** In the crystal structure of Cu_2OSeO_3, the magnetic building blocks are strong (**a**) and weak (**b**) tetrahedra. Cu(1) and Cu(2) atoms are denoted as "1" and "2", respectively. SeO_3 pyramids are shown green. **c**, the long-range exchange $J^{\mathrm{AF}}_{\mathrm{O...O}}$ runs via the O..O edge of a SeO_3 group.

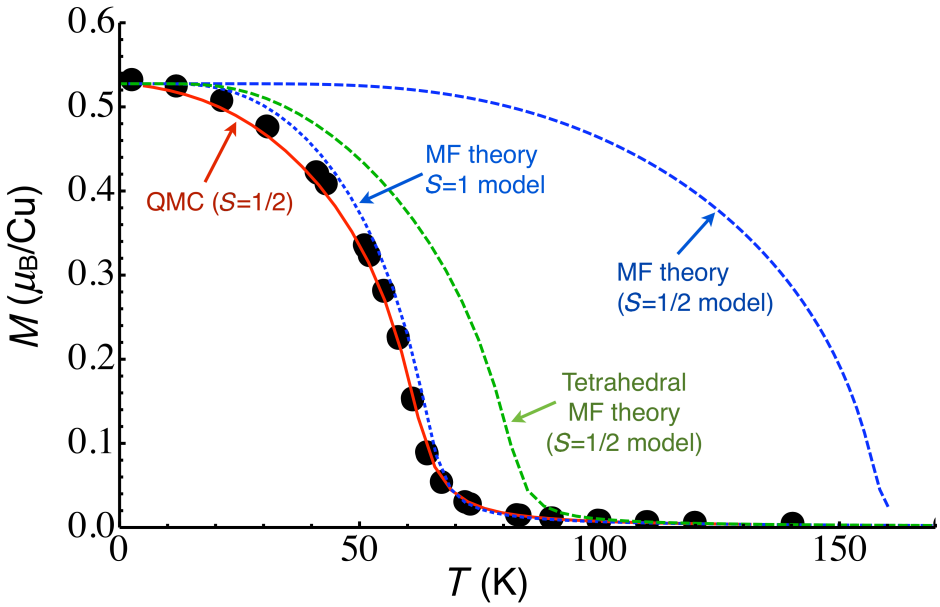

Supplementary Figure 3: **Comparison of QMC and different MF theories with the experimental magetization.** Temperature dependence of the magnetization at 0.5 T, from experiments (Ref. 1) (black symbols), QMC simulations of the microscopic $S = \frac{1}{2}$ model (red solid line, see also Figure 3), the mean-field theory in the $S = \frac{1}{2}$ model (dashed blue line), the mean-field theory in the effective $S = 1$ model (dotted blue line), and the tetrahedral mean-field theory (dashed green line).

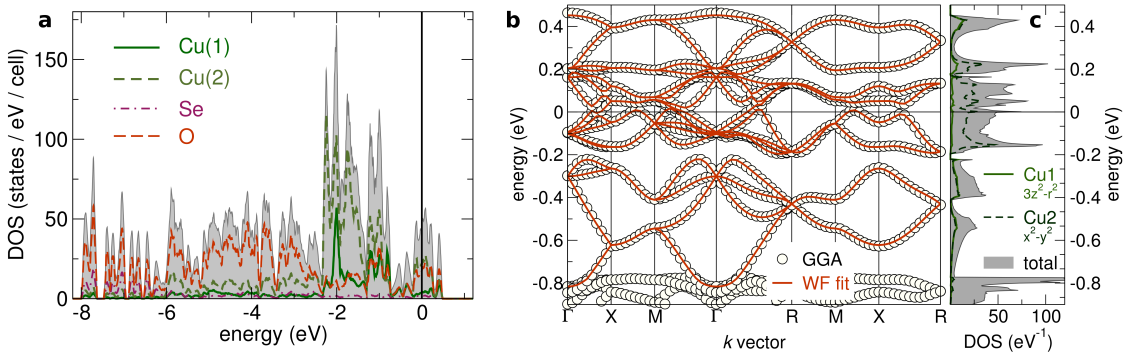

Supplementary Figure 4: **Nonmagnetic GGA band structure calculations.** **a**, GGA density of states (DOS) of the valence band of Cu_2OSeO_3. **b**, GGA band structure of Cu_2OSeO_3. The 16-bands manifold of the magnetically active states is well-reproduced by Cu-based Wannier functions (lines). The Fermi level is at zero energy. **c**, total density of states (DOS) and orbital-resolved DOS for the magnetically active Cu(1) $3d_{3z^2-r^2}$ and Cu(2) $3d_{x^2-y^2}$ states.

Supplementary Tables

Supplementary Table 1: Leading transfer integrals (hoppings) in Cu_2OSeO_3: type of Cu atoms involved in the exchange, their positions $\mathbf{r}_i$ and $\mathbf{r}_j$, their distance $d = |\mathbf{r}_i - \mathbf{r}_j|$ (in Å), transfer integrals t_{ij} (in meV), and antiferromagnetic superexchange J_{ij}^{AF} (in K). Transfer integrals are evaluated as nondiagonal elements between the Wannier functions for Cu(1) $3d_{3z^2-r^2}$ and Cu(2) $3d_{x^2-y^2}$ states. J_{ij}^{AF} is evaluated as $4t^2/U_{\mathrm{eff}}$ for $U_{\mathrm{eff}} = 4.5\,\mathrm{eV}$.

transfer integral	atoms	$\mathbf{r}_i$	$\mathbf{r}_j$	$d = \lvert\mathbf{r}_i - \mathbf{r}_j\rvert$	t_{ij}	J_{ij}^{AF}
t_W^{FM}	Cu(2)-Cu(2)	ρ_5	ρ_{12}	3.039	−55	31
t_S^{AF}	Cu(1)-Cu(2)	ρ_4	ρ_{11}	3.057	−170	298
t_S^{FM}	Cu(2)-Cu(2)	ρ_8	ρ_{15}	3.220	−31	10
t_W^{AF}	Cu(1)-Cu(2)	ρ_1	ρ_8	3.300	−106	116
$t_{\mathrm{O...O}}^{\mathrm{AF}}$	Cu(1)-Cu(2)	ρ_4	ρ_{12}	6.352	−68	48

Supplementary Notes

Supplementary Note 1

The cubic crystal structure of Cu_2OSeO_3 is formed by three different types of polyhedra: trigonal bipyramids $Cu(1)O_5$, distorted plaquettes $Cu(2)O_4$ and nonmagnetic SeO_3 pyramids. The actual positions of the magnetic Cu atoms are given in the Methods section.

Our study reveals that Cu_2OSeO_3 features two types of magnetic tetrahedra: strong tetrahedra, comprising strong magnetic couplings ($J_S^{\rm AF}$ and $J_S^{\rm FM}$), and weak tetrahedra, where the magnetic couplings are substantially weaker ($J_W^{\rm FM}$ and $J_W^{\rm AF}$). These tetrahedra also differ on the structural level: in the strong tetrahedra, $Cu(1)O_5$ and $Cu(2)O_4$ polyhedra share three common O..O edges (Supplementary Figure **2**, **a**), whereas in the weak tetrahedra, they share a common O atom, only (Supplementary Figure **2**, **b**).

The long-range magnetic coupling $J_{\rm O...O}^{\rm AF}$ is mediated by the O..O edge of SeO_3 group (Supplementary Figure **2**, **c**), which provides a substantial σ-overlap of magnetic Cu(1) $3d_{3z^2-r^2}$ and Cu(2) $3d_{x^2-y^2}$ orbitals with respective O $2p$ orbitals.

Supplementary Methods

1. DFT calculations

Nonmagnetic calculations

The initial step of our computational procedure is a nonmagnetic band structure calculation. For the nonmagnetic calculations, we used an $16\times16\times16$ k-mesh with 368 points in the irreducible wedge. LDA and GGA yield marginally different band structures, thus we restrict our analysis to the GGA. The valence band width of 8.5 eV (Supplementary Figure **4**, **a**) is similar to the related Cu^{2+} compounds. The energy range between -8 and -6 eV is dominated by Se and O states, typical for covalent Se–O bonds. The rest of the valence band is formed by Cu and O states.

The metallic spectrum contrasts with the experimentally proven insulating nature of Cu_2OSeO_3 [2]. This drawback of LDA and GGA stems from the underestimation of strong electronic correlations, inherent to the spatially confined $3d$ orbitals of Cu. The insulating state can be restored by adding the missing on-site correlations within a Hubbard model, or using the mean-field DFT+U formalism.

The magnetic properties of Cu_2OSeO_3 are ruled by the sixteen bands in the vicinity of the Fermi level (Supplementary Figure **4**, **b**). The orbital character of the magnetically active states can be analysed by projecting these bands onto a local coordinate system. In the trigonal bipyramids $Cu(1)O_5$, the z axis connects the apices, the x axes runs along one of the Cu(1)–O bonds lying in the basal plane. For Cu(2) plaquettes, the local x-axis runs along one

of the Cu(2)–O bonds, while the z-axis is perpendicular to the plaquette plane. In this way, we find that the magnetically active (half-filled) orbitals are $3z^2-r^2$ for Cu(1) and x^2-y^2 for Cu(2) (Supplementary Figure **4**, **c**). In cuprates, such an alternation of magnetically active orbitals is very scarce, it was recently suggested for the spin-1/2 frustrated magnet volborthite $Cu_3V_2O_7(OH)_2{\cdot}2H_2O$ [3].

Since the number of magnetically relevant bands (16) matches the number of Cu atoms in the unit cell, the magnetism of Cu_2OSeO_3 can be described by an effective one-orbital model within the tight-binding approximation:

$$\hat{H}_{\rm TB} = -\sum_{i>j,\sigma} t_{ij}(\hat{c}^{\dagger}_{i\sigma}\hat{c}_{j\sigma} + \hat{c}^{\dagger}_{j\sigma}\hat{c}_{i\sigma}) - \sum_{i,\sigma}\epsilon_i\,\hat{c}^{\dagger}_{i\sigma}\hat{c}_{i\sigma},$$

where t_{ij} and ϵ_i are the transfer integrals and the on-site energies, respectively. To parameterize the model, we resort to localized Wannier functions for Cu(1) $3d_{z^2-r^2}$ and Cu(2) $3d_{x^2-y^2}$ states, and evaluate the model parameters t_{ij} and ϵ_i as nondiagonal and diagonal elements, respectively (see Ref. 4 for the methodological aspects). In this way, we find that only four transfer integrals t_{ij} are larger than 40 meV: $t_S^{\rm AF}$, which couples Cu(1) and Cu(2) in the strong tetrahedra; two inequivalent couplings $t_W^{\rm FM}$ and $t_S^{\rm AF}$ in the weak tetrahedra, as well as the long-range coupling $t_{\rm O...O}^{\rm AF}$ mediated by the O...O edge of a SeO_3 pyramid.

These four terms, supplemented with the short-range coupling $t_S^{\rm FM}$ (this superexchange pathway facilitates a substantial ferromagnetic component to the respective magnetic exchange, see below), constitute a minimal basis for the microscopic magnetic model (Supplementary Table **1** and Supplementary Figure **1**, **a**.

The resulting transfer integrals can be mapped onto an effective tight-binding model, which is in turn supplemented by a Hubbard term, in order to restore the insulating ground state. In the strongly correlated limit (Coulomb repulsion $U_{\rm eff}$ dominates over electron transfer t_{ij}) and at half-filling, both well-justified for undoped cuprates, the lowest-lying (magnetic) excitations of this Hubbard model can be described by a Heisenberg model with the antiferromagnetic exchange $J_{ij}^{\rm AF} = 4t_{ij}^2/U_{\rm eff}$ [5]. The $J_{ij}^{\rm AF}$ estimates are given in Supplementary Table **1**.

In this approach, only the antiferromagnetic contribution to the magnetic exchange can be estimated. To account for the ferromagnetic contribution, which can be especially large for short-range couplings, we use DFT+U calculations.

DFT+U calculations

DFT+U calculations are a standard computational tool for orbitally-ordered insulators. In this method, the missing electronic correlations are added in the static mean-field approximation, by introducing an additional on-site Coulomb repulsion U_d and on-site Hund's exchange J_d that are applied to the d states of Cu. Such an alteration favors integer occupation numbers

and restores the insulating ground state [6, 7].

Accurate estimation of the parameters U_d and J_d is a challenging task. These on-site terms are applied to a particular manifold of states, only, which is unphysical and impedes an independent experimental estimation of the parameters. Moreover, the values of U_d and J_d can vary depending on the way the d orbitals are defined in the code (basis dependence).

Here, to estimate the on-site repulsion and exchange, we performed auxiliary constrained LDA calculations using the `TB-LMTO-ASA` code [8]. Following the calculational procedure from Ref. 9, we obtain $U_d = 10.5\,\text{eV}$ and $9.5\,\text{eV}$ for Cu(1) and Cu(2), respectively. J_d is very close to $1\,\text{eV}$ for both Cu atoms. We adopt these values and perform DFT+U calculations using the *vasp* code. For the double-counting correction, we use the fully localized limit [10].

A standard way to evaluate exchange integrals are total energy DFT+U calculations for magnetic supercells. In the case of Cu_2OSeO_3, the crystallographic cell (16 Cu atoms) suffices to evaluate all five relevant exchanges. Numerical estimates for the magnetic exchanges J_{ij} are obtained by mapping the DFT+U total energies onto a classical Heisenberg model:

$$E = E_0 + \sum_{\{ij\}} J_{ij}\ \mathbf{S_i} \cdot \mathbf{S_j}\ , \tag{1}$$

where $\{ij\}$ labels all relevant interaction bonds. In a scalar-relativistic calculation, the spin-orbit coupling is neglected, thus only collinear configurations can be treated: $\mathbf{S_i} \cdot \mathbf{S_j}$ is either $\frac{1}{4}$ or $-\frac{1}{4}$. The exchange integrals J_{ij} (Table 1) are evaluated as solutions to a redundant system of 15 linear equations of the type Eq. (1).

Full-relativistic DFT+U calculations

The Dzyaloshinskii-Moriya couplings are estimated by mapping the full-relativistic DFT+U total energies for different staggered magnetic configurations onto the classical bilinear exchange model:

$$E' = \sum_{i>j} \sum_{\alpha,\beta} \mathbf{M}_{\alpha,\beta} \mathbf{S}_i^{\alpha} \mathbf{S}_j^{\beta} \quad (\alpha, \beta = x, y, z), \tag{2}$$

where all anisotropic exchange terms are comprised in the 3×3 matrix M. The antisymmetric part of this matrix contains the components of the Dzyaloshinskii-Moriya vector $\mathbf{D}$:

$$\begin{pmatrix} 0 & D_z & -D_y \\ -D_z & 0 & D_x \\ D_y & -D_x & 0 \end{pmatrix} \tag{3}$$

To estimate the matrix elements of $\mathbf{M}$, we use the four-state mapping method developed by Xiang and coworkers [11]. The total energies are calculated using full-relativistic DFT+U implemented in vasp code on a $2\times2\times2$ k-mesh. The resulting energies were carefully checked for convergence. The resulting DM anisotropies are provided in Supplementary Table 1.

2. QMC simulations

To verify and refine the DFT+U estimates for the isotropic exchange couplings, we performed Quantum Monte Carlo (QMC) simulations of the temperature dependence of the magnetic susceptibility χ^* (for the paramagnetic state) and the magnetization M^* (for the magnetically ordered state), as well as finite-size dependence of the spin stiffness (for the magnetic ordering temperature T_C).

Simulations of $\chi^*(T^*)$ were done using the code `loop` (Ref. 12) from the software package `ALPS` version 1.3.[13] Simulations were performed on finite lattices of 8192 spins $S = \frac{1}{2}$ using periodic boundary conditions, with 40 000 sweeps for thermalization and 400 000 sweeps after thermalization. The simulated curves are fitted to the experimental $\chi(T)$ dependence (digitized data from Ref. 2) using the following expression:

$$\chi(T) = \frac{N_A g^2 \mu_B^2}{k_B J} \cdot \chi^* \left(\frac{T}{k_B J} \right). \tag{4}$$

We adopted the experimental value $g = 2.11$ measured using ESR [14]. Thus, the only free parameter is the overall energy scale J. The fit yields $J = 170\,\mathrm{K}$, slightly exceeding the DFT+U estimate for J_S^{AF} (149.2 K). Thus, we scaled all DFT+U estimates for the isotropic couplings by a factor of 1.14 to obtain the correct experimental energy scale, see Table 1.

In the next step, we verified the magnetic ordering temperature. To this end, we simulated spin stiffness ρ_S for different finite lattice sizes, and performed a finite-size scaling. The quantity $\rho_S L$ is independent of the linear dimension L of the finite lattice at the ordering temperature [15]. Thus, the crossing point in Figure 3 (**b**) directly yields $T/J \simeq 0.34$. Adopting $J = 170\,\mathrm{K}$, we obtain $T_C \simeq 58\,\mathrm{K}$, in excellent agreement with the experimental $T_C^{\mathrm{exp}} = 60\,\mathrm{K}$ [2, 16].

Finally, to address the magnetically ordered state, we simulated the temperature dependence of the magnetization in different magnetic fields. These simulations were performed using the code `dirloop_sse` (Ref. 17) from the software package `ALPS` version 1.3 [13]. The simulated $M^*(T^*)$ curves were scaled using the following expression

$$M(T) = g M^* \left(\frac{T^*}{k_B J} \right), \tag{5}$$

adopting $J = 170\,\mathrm{K}$ obtained from the fit to the $\chi(T)$ data and the experimental $g = 2.11$ [14]. In this zero-parameter fit, we obtain excellent agreement with the experimental $M(T)$ measured in magnetic fields of 0.5, 4.5, and 14 Tesla, see Figure 3, **a**.

Comparison with previous *ab initio* studies — The ab initio results for the exchange constants reported by Yang *et al.* (Ref. 18) are generally much smaller than our estimates (The exchange couplings reported in Ref. 18 are: $J_S^{\mathrm{AF}} = 75.82\,\mathrm{K}$, $J_W^{\mathrm{AF}} = 10.44\,\mathrm{K}$, $J_S^{\mathrm{FM}} = -42.86\,\mathrm{K}$, $J_W^{\mathrm{FM}} = -13.14\,\mathrm{K}$, and $J_{\mathrm{O\ldots O}}^{\mathrm{AF}} = 11.42\,\mathrm{K}$). For example, the dominant antiferromagnetic coupling

is 75.82 K in Ref. 18, which is more than two times smaller than our result of ~ 170 K. At the mean-field level, the parameters of Ref. 18 give $T_{\rm C}^{{\rm MF},S=\frac{1}{2}} \simeq 58.55$ K, which is very close to $T_{\rm C}^{\rm exp} \simeq 60\,{\rm K}$ [2, 16]. However, the presence of two well-separated exchange energy scales in the problem gives rise to strong quantum-mechanical correlations that are not captured by the mean-field theory. As shown in the main paper, one of the main consequences of these correlations is that the effective energy scale responsible for the ordering is much smaller than the microscopic exchange couplings. So in contrast to the mean-field theory, the exchange parameters of Ref. 18 actually give a number which is about three times smaller than $T_{\rm C}^{\rm exp}$. This can be seen e.g. by using the mean-field theory of the effective $S = 1$ model, which captures most of the quantum-mechanical correlations, yielding (see 13 below) $T_{\rm C}^{{\rm MF},S=1} \simeq 18.23\,{\rm K}$, that drastically underestimates the experimental $T_{\rm C}$.

3. Mean-field theories

One of the central aspects of Cu_2OSeO_3 that derives from the effective, strong coupling picture is that only the weak exchange couplings are essential for the basic helimagnetism below $T_{\rm C}$. This aspect can be demonstrated more explicitly by considering three mean-field (MF) treatments of the problem: a single-site MF in the original spin-1/2 model, a single-site MF in the effective spin-1 model, and a tetrahedral MF treatment of the original spin-1/2 problem. In all of them we disregard the DM couplings since they are much smaller than the exchange couplings and so they are not expected to affect much the T-dependence of the magnetization (at high enough T) or the value of T_C.

Single-site mean-field theory in the bare $S = \frac{1}{2}$ model

The single-site mean-field theory in the bare $S = \frac{1}{2}$ model has been worked out in Ref. 16 for a simplified model with only two bare exchange couplings. Here we repeat the same steps using the present set of exchange couplings from ab initio calculations. We begin by writing down the mean-field Hamiltonian for an isolated spin $S = \frac{1}{2}$ in a local magnetic field. Given that there are two types of Cu sites we consider two different local fields $\mathbf{B}_1$ and $\mathbf{B}_2$:

$$\mathcal{H}_{\rm Cu(1)}^{{\rm MF},S=\frac{1}{2}} = -\mathbf{B}_1 \cdot \mathbf{S}_{\rm Cu(1)}, \quad \mathcal{H}_{\rm Cu(2)}^{{\rm MF},S=\frac{1}{2}} = -\mathbf{B}_2 \cdot \mathbf{S}_{\rm Cu(2)} \ . \tag{6}$$

Assuming $\mathbf{B}_{1,2} = B_{1,2}\mathbf{z}$, the solution for the magnetizations at temperature T are given by the well known formula:

$$\langle S^z_{\rm Cu(1)} \rangle = \frac{1}{2} \tanh(\beta B_1/2), \quad \langle S^z_{\rm Cu(2)} \rangle = \frac{1}{2} \tanh(\beta B_2/2) \ , \tag{7}$$

where $\beta = 1/(k_B T)$. To proceed we must relate the local fields to the local magnetizations by examining the connectivities of the various couplings. Each Cu(1) site interacts with nine Cu(2) spins: three via $J_S^{\rm AF}$, plus three via $J_{\rm W}^{\rm AF}$, plus three via $J_{\rm O...O}^{\rm AF}$. On the other hand,

each Cu(2) spin interacts with four Cu(2) spins (two via $J_{\rm S}^{\rm FM}$ plus two via $J_{\rm W}^{\rm FM}$), and three Cu(1) spins (one via $J_{\rm S}^{\rm AF}$, plus one via $J_{\rm W}^{\rm AF}$, plus one via $J_{\rm O...O}^{\rm AF}$). Therefore

$$B_1 = B_0 - j_{12}\langle S^z_{\rm Cu(2)}\rangle, \quad B_2 = B_0 - j_{21}\langle S^z_{\rm Cu(1)}\rangle - j_{22}\langle S^z_{\rm Cu(2)}\rangle \ , \tag{8}$$

where B_0 is the external magnetic field, and $j_{21} \equiv J_{\rm S}^{\rm AF} + J_{W}^{\rm AF} + J_{\rm O...O}^{\rm AF} > 0$, $j_{12} \equiv 3j_{21}$, and $j_{22} \equiv 2(J_{\rm S}^{\rm FM} + J_{\rm W}^{\rm FM}) < 0$. Replacing Eqs. (8) into Eqs. (7) gives two non-linear equations which must be solved self-consistently in order to obtain the magnetizations as a function of T and B_0. The full T-dependence of the total magnetization is shown in Supplementary Figure **3**.

Within this mean-field approximation, the transition temperature $T_{\rm C}^{{\rm MF},S=\frac{1}{2}}$ can be found by setting $B_0 = 0$ and expanding the right hand side of Eqs. (7) for small $B_{1,2}$ (which is equivalent to the region of small $S^z_{\rm Cu(1)}$ and $S^z_{\rm Cu(2)}$), which yields

$$T_{\rm C}^{{\rm MF},S=\frac{1}{2}} = \frac{1}{4}\left(\frac{|j_{22}|}{2} + \sqrt{\left(\frac{j_{22}}{2}\right)^2 + j_{12}j_{21}}\right) \ . \tag{9}$$

Using our ab initio couplings we get a numerical value of $T_{\rm C}^{{\rm MF},S=\frac{1}{2}} \simeq 0.919 J_S^{\rm AF} \simeq 156.23$ K (see also Supplementary Figure **3**), which is more than two times larger than the experimental value of $T_{\rm C}^{\rm exp} \simeq 60\,{\rm K}$. As explained in the main body of the paper, the reason for this large discrepancy is rooted in the fact that the elementary magnetic degrees of freedom that order at $T_{\rm C}$ are not the bare $S = \frac{1}{2}$ Cu^{2+} spins but the effective $S = 1$ entities of each strong tetrahedron. As we show below, doing the mean-field decoupling in the effective $S = 1$ model delivers a much better estimate for $T_{\rm C}$.

Single-site mean-field theory in the effective $S = 1$ model

The single-site mean-field theory in the effective $S = 1$ model is based on the solution of the quantum-mechanical problem of an isolated spin $S = 1$ in a magnetic field $\mathbf{B}$,

$$\mathcal{H}^{{\rm MF},S=1} = -\mathbf{B}\cdot\mathbf{S} \ . \tag{10}$$

Taking again $\mathbf{B} = B\mathbf{z}$, the solution for the magnetization at temperature T is given by the $S = 1$ Brillouin function:

$$\langle S^z\rangle = \mathcal{B}_{S=1}(\beta B) = \frac{2\sinh(\beta B)}{1 + 2\cosh(\beta B)} \ . \tag{11}$$

Using the fact that each $S = 1$ site has six nearest neighbors and six next-nearest neighbors and replacing

$$B = B_0 - 6(J_1 + J_2)\langle S^z\rangle \tag{12}$$

in Eq. (11), where B_0 is the external magnetic field, gives a non-linear equation which must be solved self-consistently to find $\langle S^z \rangle$ as a function of T and B_0. The full T-dependence of the total magnetization is shown in Supplementary Figure **3**.

In this mean-field theory, the transition temperature $T_{\rm C}^{{\rm MF},S=1}$ can be found by setting $B_0 = 0$ and expanding the right hand side of Eq. (11) around the limit of small B (or small $\langle S^z \rangle$). We find

$$T_{\rm C}^{{\rm MF},S=1} = -4(J_1 + J_2). \tag{13}$$

Using our values for J_1 and J_2 we find $T_{\rm C}^{{\rm MF},S=1} = 64.7$ K, which is rather close to the experimental value, see also Supplementary Figure **3**.

Tetrahedral mean-field (TMF) theory for $S = 1/2$

The above single-site mean-field theory in the effective $S = 1$ model has two main problems, one at very high T and another at low T. At very high T, we expect a paramagnetic behavior of isolated $S = \frac{1}{2}$ spins, whereas in the spin-1 model the basic building blocks (effective triplets) retain their integrity at all temperatures. The second problem of the S=1 mean-field theory is related to the spin-mixing effect discussed in the main paper. Namely, the fact that the local exchange field exerted from the neighboring tetrahedra admix a finite $S = 2$ amplitude into the triplet ground state, leading to renormalized values for the local spin moments at zero temperature (Table 2).

To account for these two problems we solve the tetrahedral mean field (TMF) Hamiltonian discussed in the main text (see Methods section) at finite temperatures. This can be done numerically using e.g. an iterative self-consistent procedure. The full T-dependence of the total magnetization is shown in Supplementary Figure **3** along with the previous mean-field theories, QMC results on finite-size clusters as well as experimental data at 0.5 Tesla. Using our ab initio values for the exchange couplings we find the transition temperature $T_c^{{\rm TMF},S=\frac{1}{2}} \simeq 0.47 J_S^{\rm AF} \simeq 79.9$ K. So, although the tetrahedral mean-field theory captures better the $T = 0$ physics (local magnetizations, spin-mixing effect, etc) compared to the $S = 1$ mean-field theory, the latter overestimates $T_{\rm C}$ much less.

Cubic anisotropy from magneto-electric effect

As mentioned in the main text, one source of the cubic anisotropy constant $\mathcal{K}_1$ may come from the magnetoelectric (ME) coupling. Here we show that the actual numerical value of that contribution, as extracted from experimental ME data, is too small to be the relevant source of this anisotropy.

The ME coupling in Cu_2OSeO_3 has the following form[19]:

$$V_{\rm ME}(\mathbf{P}, \mathbf{M}) = \lambda_{\rm ME} \left(P_x M_y M_z + P_y M_z M_x + P_z M_x M_y \right) , \tag{14}$$

where $\mathbf{P}$ is the electric polarization density and $\lambda_{\rm ME}$ is the ME coupling constant. Integrating out the polarization gives[19]:

$$\mathbf{P}/\chi_e = \lambda_{\rm ME}\left(M_yM_z, M_zM_x, M_xM_y\right) \ , \tag{15}$$

where χ_e is the dielectric susceptibility. Replacing in Eq. (14) gives an extra contribution to the energy

$$V'_{\rm ME}(\mathbf{M}) = \lambda^2_{\rm ME}\chi_e\left[(M_yM_z)^2 + (M_zM_x)^2 + (M_xM_y)^2\right] \ , \tag{16}$$

which identifies the ME contribution to $\mathcal{K}_1$ to be $\mathcal{K}_1^{\rm ME} = \lambda^2_{\rm ME}\chi_e$. Note that the sign of the prefactor is positive, regardless of the sign of the coupling constant $\lambda_{\rm ME}$, meaning that this contribution favors the cubic [100] axes as the easy axis and the [111] axes as the hard axes, in agreement with experiment.[19, 20] However, as we show below, $\mathcal{K}_1^{\rm ME}$ is too small compared to the value of $\mathcal{K}_1 \simeq 1.0\times10^{-16}\,\frac{\rm J\,m}{\rm A^4}$, which was found by fitting the magnetization process along the (100) direction (see main text).

The dielectric constant can be extracted from the dielectric measurements of Figure 5 of [19], which at low temperatures give

$$\chi_e \simeq 6\,\epsilon_0 = 5.31251\times10^{-11}\ \frac{\rm A^2\,s^2}{\rm J\,m}\,. \tag{17}$$

Next, we use the experimental polarization data of Figure 17 of [19] to extract the low-T polarization $P^\star$ at the field-aligned ferrimagnetic plateau state for the orientation with the maximum response ($\theta = 45^\circ$):

$$P^\star \simeq 13.75\ \mu{\rm C/m^2}\,. \tag{18}$$

The coupling constant $\lambda_{\rm ME}$ then follows from formula (19) (in the notation of [19], $\lambda_{\rm ME} = \xi_+/2$):

$$\lambda_{\rm ME} = \frac{P^*}{\chi_e\, M^2_{\rm sat(0)}} \simeq 2.1\times10^{-5}\,\frac{\rm J\,m}{\rm A^3\,s}\,, \tag{19}$$

where we used $M_{\rm sat}(0) = 111.348$ kA/m, for the low-temperature value of the magnetization at the plateau. In turn, this gives

$$\mathcal{K}_1^{\rm ME} = \lambda^2_{\rm ME}\,\chi_e \simeq 2.3\times10^{-20}\,\frac{\rm J\,m}{\rm A^4}\,. \tag{20}$$

which is about four orders of magnitude smaller than the above given value of $\mathcal{K}_1$. This shows that the cubic anisotropy $\mathcal{K}_1$ does not originate in the ME coupling.

4. Lattice Summations

Here we give the explicit forms of a number of lattice summations that appear in the derivation of the effective model in the trillium lattice. In what follows $\langle ij\rangle$ and $\langle\langle ij\rangle\rangle$ denote NN and

NNN of the trillium lattice, respectively. We begin with the sums that are needed for the exchange portion of the energy density.

$$\sum_{\langle ij\rangle}\eta_{i,\mu}=\sum_{\langle\langle ij\rangle\rangle}\eta_{i,\mu}=-\sum_{\langle ij\rangle}\eta_{j,\mu}=-\sum_{\langle\langle ij\rangle\rangle}\eta_{j,\mu}=(8,4,0),\ \ \sum_{\langle ij\rangle}\eta_{i,\mu}\eta_{j,\nu}=\sum_{\langle\langle ij\rangle\rangle}\eta_{i,\mu}\eta_{j,\nu}=\begin{pmatrix}-4&0&-4\\0&-4&0\\4&0&-4\end{pmatrix}_{\mu\nu}$$

$$\Rightarrow\quad \sum_{\mu,\nu=1}^{3}\sum_{\langle ij\rangle}\eta_{i\mu}\eta_{j\nu}\mathbf{L}_\mu\cdot\mathbf{L}_\nu=\sum_{\mu,\nu=1}^{3}\sum_{\langle\langle ij\rangle\rangle}\eta_{i\mu}\eta_{j\nu}\mathbf{L}_\mu\cdot\mathbf{L}_\nu=-4(\mathbf{L}_1^2+\mathbf{L}_2^2+\mathbf{L}_3^2)$$

$$\sum_{\langle ij\rangle}(\partial_j-\partial_i)=2(7-8y)\partial_z+8(1-y)\partial_y,\qquad \sum_{\langle\langle ij\rangle\rangle}(\partial_j-\partial_i)=2(9-8y)\partial_z+8(1-y)\partial_y$$

$$\sum_{\langle ij\rangle}(\eta_{i\mu}-\eta_{j\mu})(\partial_j-\partial_i)=4(7-8y)\{\partial_z,\partial_y,\partial_x\},\quad \sum_{\langle\langle ij\rangle\rangle}(\eta_{i\mu}-\eta_{j\mu})(\partial_j-\partial_i)=4(9-8y)\{\partial_z,\partial_y,\partial_x\}$$

$$\sum_{\langle ij\rangle}\frac{1}{2}(\partial_j-\partial_i)^2=(13-28y+16y^2)\nabla^2,\qquad \sum_{\langle\langle ij\rangle\rangle}\frac{1}{2}(\partial_j-\partial_i)^2=(21-36y+16y^2)\nabla^2$$

$$\Rightarrow\sum_{\langle ij\rangle\cup\langle\langle ij\rangle\rangle}\frac{1}{2}J_{ij}(\partial_j-\partial_i)^2=\mathcal{J}\nabla^2\ ,\quad \text{where } \mathcal{J}\equiv(13-28y+16y^2)J_1+(21-36y+16y^2)J_2$$

$$\sum_{\langle ij\rangle}\frac{1}{2}(\eta_{i\mu}+\eta_{j\mu})(\partial_j-\partial_i)^2=8(3-7y+4y^2)\{\partial_x\partial_y,\partial_x\partial_z,\partial_y\partial_z\},$$
$$\sum_{\langle\langle ij\rangle\rangle}\frac{1}{2}(\eta_{i\mu}+\eta_{j\mu})(\partial_j-\partial_i)^2=8(5-9y+4y^2)\{\partial_x\partial_y,\partial_x\partial_z,\partial_y\partial_z\}\ .$$

Similarly for the DM energy we shall need the following sums:

$$\sum_{\langle ij\rangle}\mathbf{D}_{ij}(\eta_{j\mu}-\eta_{i\mu})=-8(d_2+d_3)\{\mathbf{e}_z,\mathbf{e}_y,\mathbf{e}_x\},\quad \sum_{\langle\langle ij\rangle\rangle}\mathbf{D}_{ij}(\eta_{j\mu}-\eta_{i\mu})=-8(d_2'+d_3')\{\mathbf{e}_z,\mathbf{e}_y,\mathbf{e}_x\}\ ,$$
$$\sum_{\mu,\nu=1}^{3}\sum_{\langle ij\rangle}\eta_{i\mu}\eta_{j\nu}\mathbf{D}_{ij}\cdot\mathbf{L}_\mu\times\mathbf{L}_\nu=-8(d_2-d_3)[(\mathbf{L}_1\times\mathbf{L}_2)^x+(\mathbf{L}_2\times\mathbf{L}_3)^z+(\mathbf{L}_3\times\mathbf{L}_1)^y]\ ,$$
$$\sum_{\mu,\nu=1}^{3}\sum_{\langle\langle ij\rangle\rangle}\eta_{i\mu}\eta_{j\nu}\mathbf{D}_{ij}\cdot\mathbf{L}_\mu\times\mathbf{L}_\nu=-8(d_2'-d_3')[(\mathbf{L}_1\times\mathbf{L}_2)^x+(\mathbf{L}_2\times\mathbf{L}_3)^z+(\mathbf{L}_3\times\mathbf{L}_1)^y]\ ,$$

$$\sum_{\langle ij\rangle}\mathbf{D}_{ij}(\partial_j-\partial_i)=-\mathcal{D}(\partial_x,\partial_y,\partial_z),$$

where $\mathcal{D}\equiv 2[d_1+d_2(-3+4y)+4d_3(-1+y)]+2[d_1'+d_2'(-5+4y)+4d_3'(-1+y)]$.

$$\sum_{\langle ij\rangle\cup\langle\langle ij\rangle\rangle} \mathbf{D}_{ij}(\eta_{i\mu}+\eta_{j\mu})(\partial_j-\partial_i) = \begin{cases} (q\partial_y, r\partial_x, 0), & \text{if } \mu=1 \\ (r\partial_z, 0, q\partial_x), & \text{if } \mu=2 \\ (0, q\partial_z, r\partial_y), & \text{if } \mu=3 \end{cases}$$

where $q=-16(d_2+d_2')(-1+y)$ and $r=4d_3(3-4y)+4d_3'(5-4y)$.

$$\sum_{\langle ij\rangle\cup\langle\langle ij\rangle\rangle} \mathbf{D}_{ij}(\partial_j-\partial_i)^2 \;=\; \Big(\Gamma_x^{xy}\partial_x\partial_y+\Gamma_x^{xz}\partial_x\partial_z,\; \Gamma_y^{xx}\partial_x^2+\Gamma_y^{yy}\partial_y^2+\Gamma_y^{zz}\partial_z^2+\Gamma_y^{yz}\partial_y\partial_z,$$
$$\Gamma_z^{xx}\partial_x^2+\Gamma_z^{yy}\partial_y^2+\Gamma_z^{zz}\partial_z^2+\Gamma_z^{yz}\partial_y\partial_z\Big)\;,$$

where

$$\begin{aligned}
&\Gamma_x^{xy}=8(-1+y)[d_2(-3+4y)+d_2'(-5+4y)],\\
&\Gamma_x^{xz}=8(-1+y)[d_1+d_1'+d_3(-3+4y)+d_3'(-5+4y)],\\
&\Gamma_y^{xx}=d_3(3-4y)^2+d_3'(5-4y)^2,\;\; \Gamma_y^{yy}=16(d_3+d_3')(-1+y)^2,\;\; \Gamma_y^{zz}=d_3+d_3',\\
&\Gamma_y^{yz}=2(-3+4y)[d_1+4d_2(-1+y)]+2(-5+4y)[d_1'+4d_2'(-1+y)],\\
&\Gamma_z^{xx}=16(d_2+d_2')(-1+y)^2+d_3+d_3',\;\; \Gamma_z^{yy}=d_2+d_2'+(3-4y)^2d_3+(5-4y)^2d_3',\\
&\Gamma_z^{zz}=d_2(3-4y)^2+d_2'(5-4y)^2+16(d_3+d_3')(-1+y)^2,\\
&\Gamma_z^{yz}=8(d_1+d_1')(-1+y)\;.
\end{aligned}$$

Supplementary References

[1] M. Belesi et al., Magnetic properties of the magnetoelectric compound Cu_2OSeO_3: Magnetization and ^{77}Se NMR study, J. Phys.: Conf. Ser. **303**, 012069 (2011).

[2] J.-W. G. Bos, C. V. Colin and T. T. M. Palstra, Magnetoelectric coupling in the cubic ferrimagnet Cu_2OSeO_3, Phys. Rev. B **78**, 094416 (2008).

[3] O. Janson, J. Richter, P. Sindzingre and H. Rosner, Coupled frustrated quantum spin-1/2 chains with orbital order in volborthite $Cu_3V_2O_7(OH)_2{\cdot}2H_2O$, Phys. Rev. B **82**, 104434 (2010).

[4] H. Eschrig and K. Koepernik, Tight-binding models for the iron-based superconductors, Phys. Rev. B **80**, 104503 (2009).

[5] P. W. Anderson, New approach to the theory of superexchange interactions, Phys. Rev. **115**, 2 (1959).

[6] V. I. Anisimov, J. Zaanen and O. K. Andersen, Band theory and Mott insulators: Hubbard U instead of Stoner I, Phys. Rev. B **44**, 943–954 (1991).

[7] E. R. Ylvisaker, W. E. Pickett and K. Koepernik, Anisotropy and magnetism in the LSDA+U method, Phys. Rev. B **79**, 035103 (2009).

[8] O. K. Andersen and O. Jepsen, Explicit, first-principles tight-binding theory, Phys. Rev. Lett. **53**, 2571–2574 (1984).

[9] O. Gunnarsson, O. K. Andersen, O. Jepsen and J. Zaanen, Density-functional calculation of the parameters in the Anderson model: Application to Mn in CdTe, Phys. Rev. B **39**, 1708–1722 (1989).

[10] M. T. Czyżyk and G. A. Sawatzky, Local-density functional and on-site correlations: The electronic structure of La_2CuO_4 and $LaCuO_3$, Phys. Rev. B **49**, 14211–14228 (1994).

[11] H. Xiang, C. Lee, H.-J. Koo, X. Gong and M.-H. Whangbo, Magnetic properties and energy-mapping analysis, Dalton Trans. **42**, 823–853 (2013).

[12] S. Todo and K. Kato, Cluster algorithms for general-S quantum spin systems, Phys. Rev. Lett. **87**, 047203 (2001).

[13] A. Albuquerque et al., The ALPS project release 1.3: open-source software for strongly correlated systems, J. Magn. Magn. Mater. **310**, 1187–1193 (2007).

[14] A. Larrańaga, J. L. Mesa, L. Lezama, J. L. Pizarro, M. I. Arriortua and T. Rojo, Supercritical hydrothermal synthesis of $Cu_2O(SeO_3)$: Structural characterization, thermal, spectroscopic and magnetic studies, Mater. Res. Bull. **44**, 1–5 (2009).

[15] P. Sengupta, A. W. Sandvik and R. R. P. Singh, Specific heat of quasi-two-dimensional antiferromagnetic Heisenberg models with varying interplanar couplings, Phys. Rev. B **68**, 094423 (2003).

[16] M. Belesi et al., Ferrimagnetism of the magnetoelectric compound Cu_2OSeO_3 probed by ^{77}Se NMR, Phys. Rev. B **82**, 094422 (2010).

[17] A. W. Sandvik, Stochastic series expansion method with operator-loop update, Phys. Rev. B **59**, R14157–R14160 (1999).

[18] J. H. Yang et al., Strong Dzyaloshinskii-Moriya interaction and origin of ferroelectricity in Cu_2OSeO_3, Phys. Rev. Lett. **109**, 107203 (2012).

[19] M. Belesi, I. Rousochatzakis, M. Abid, U. K. Rößler, H. Berger and J.-Ph. Ansermet, Magnetoelectric effects in single crystals of the cubic ferrimagnetic helimagnet Cu_2OSeO_3, Phys. Rev. B **85**, 224413 (2012).

[20] T. Adams et al., Long-wavelength helimagnetic order and skyrmion lattice phase in Cu_2OSeO_3, Phys. Rev. Lett. **108**, 237204 (2012).